MINISTERIO
DE MEDIO AMBIENTE

SUBSECRETARÍA

DIRECCIÓN GENERAL
DEL INSTITUTO NACIONAL
DE METEOROLOGÍA

Nota Técnica número 4
del Servicio de Variabilidad y Predicción
del Clima (INM)

TROPOSPHERIC INTRASEASONAL WESTWARD-TRAVELING WAVES IN THE EURO-ATLANTIC REGION

Nota técnica nº 4
del Servicio de Variabilidad
y Predicción del Clima del I.N.M

Edita: Centro de Publicaciones
Secretaría General Técnica
Ministerio de Medio Ambiente ©

I.S.B.N.: 84-8320-109-7
NIPO: 310-00-050-3
Depósito Legal: M-20697-2000

Imprime: Centro de Publicaciones

Impreso en papel reciclado

TROPOSPHERIC INTRASEASONAL WESTWARD-TRAVELING WAVES IN THE EURO-ATLANTIC REGION

Nota Técnica núm. 4
Servicio de Variabilidad y Predicción del Clima
Instituto Nacional de Meteorología

F. JAVIER DOBLAS-REYES
ASUNCIÓN PASTOR SAAVEDRA
MARÍA JESÚS CASADO CALLE

TROPOSPHERIC INTRASEASONAL WESTWARD-TRAVELING WAVES IN THE EURO-ATLANTIC REGION

F.J. Doblas-Reyes[1] , Asunción Pastor Saavedra[2] , María Jesús Casado Calle[2]

(1) Centro de Astrobiología, INTA, Ctra de Ajalvir km4, 28850 Torrejón de Ardoz, Madird

(2) Instituto Nacional de Meteorología, Camino de las Moreras s/n Ciudad Universitaria 28040 Madrid

List of contents

Abstract

To get an insight into the low-frequency atmospheric variability over the Euro-Atlantic region, a space-time spectral analysis has been applied to two datasets: ERA (ECMWF reanalyses) and a simulation with a climate version of the atmospheric general circulation model ARPEGE-IFS. Each dataset consists on gridded daily 500 hPa geopotential height of 14 winters (1979/1980 to 1992/1993).

The model is still exhibiting less variability than the real atmosphere, mainly north of 50°N. Some noticeable features that appear in the simulation are the different behaviour of the errors among the synoptic and planetary-scale perturbations, the low variance of standing planetary waves and, especially, the presence of the planetary-scale westward traveling waves, not captured in previous works except in very high resolution versions. This represents a clear improvement, which turns out to be a very important matter in model development.

INTRODUCTION

The causes of atmospheric low-frequency variability (i.e, variability of planetary scales of 10 days up to several years) at midlatitudes are not well known. There are speculations about their origin, which can be classified into two broad types of mechanisms. The first of these is an atmospheric response to anomalous external forcing through low-frequency oscillations of its boundary condition (e.g. anomalies in sea surface temperatures (SST)). The second category is the internal dynamics of the atmosphere. A number of possible processes are found in this category: the feedback of high frequency eddies onto the low-frequency components of the flow, so-called weather regimes, in which high and low-frequency variability equilibrate, the existence of nearly steady states, including modons and blocked flow, barotropic instability of the time-mean flow, traveling free Rossby waves etc.

It is believed that the mechanisms in the second category can work in the absence of any anomalous external forcing. In most circumstances the second category appears to dominate the first in the northern-hemisphere midlatitudes. Recently, D´Andrea and Vautard (2000) have confirmed that the low-frequency variability in the Euro-Atlantic region is to a certain extent sustained by internal dynamics and relies less on the boundary conditions than in other regions of the northern hemisphere.

Some studies have been concerned with the investigation of the horizontal and vertical structure of waves with various space and time scales. It is important in weather forecasting to predict transient planetary waves correctly (Hayashi and Golder, 1993) since they account for the intermittent amplification and phase shift of quasi-stationary waves. Pratt and Wallace (1976) showed that, after averaging over bands of wavenumber and frequency, there are two basic types of midlatitude winter season traveling waves which predominate in the Northern Hemisphere. One has the structure of a barotropic external mode with significant amplitude at the surface and little phase variation with height and moves westward. The other moves eastward, the amplitude increases rapidly with

altitude from small values at the surface and has substantial westward phase tilt with altitude. Much attention has been given to the westward traveling waves in the Northern Hemisphere where westward moving planetary scale waves seem to be more noticeable (Mechoso and Hartmann, 1982). In the present study, attention is focused on the behaviour of the low-frequency westward traveling (or retrograde) waves in the northern latitudes of the Atlantic. These disturbances are generated by two different mechanisms: by the tropical-extratropical interaction which would give rise to the highest-frequency westward waves observed southward of 45°N, and by a dynamical effect, typical of the mid-latitudes which would be associated to blocking. As these disturbances can have relatively large amplitude (Speth and Madden, 1982), it is important to know as much as possible about their behaviour in order to better understand time variations in the large-scale circulation. The framework through which we will attempt to achieve this aim is the space-time spectral analysis technique (Hayashi 1971, 1982; Pratt 1976).

DATA SETS

The study is based on two datasets consisting of gridded daily 500 hPa geopotential heights (12 GMT) of 14 winters (1979/1980 to 1992/1993). The two sets are the reanalyses of the European Centre for Medium Range Forecasts (ECMWF), CEP henceforth, and a 14 year integration of the ARPEGE model.

The ECMWF reanalysis project (ERA) has used a frozen version of their analysis-forecast system, at a triangular spectral truncation of T106 with 31 levels in the vertical, to perform data assimilation, using data from 1979 to 1993.

The ARPEGE (Action de Recherche, Petite Echelle, Grande Echelle) GCM was adapted from the numerical weather prediction model developed jointly by Météo-France and the ECMWF. The recently developed version number 3 has been used in this study. The basic climate versions are described in Déqué et al. (1994) (version 0), Déqué and Piedelievre (1995) (version 1) and in Doblas-Reyes and Déqué (1998) (version 2). This new version shows some differences compared with the previous ones. As far as dynamics is concerned, the use of a

semiLagrangian advection scheme which allows for the use of a linear grid, instead of a Gaussian one. Some new physical parametrizations are also included: a new stratiform cloud and precipitation schemes, the prescription of the vertical mixing length making use of a diagnosed mixing layer height, a more realistic way of treating convection effects, the variation through the vertical of the cloud cover. Finally, improvements in the ISBA surface and vegetation schemes have also been taken into account.

The simulation has been carried out with a discretization of 41 levels in the vertical and a spectral truncation of T63. It was initiated with 5 years of relaxation of the system and then the model has been integrated for 17 years. Prescribed daily SST were linearly interpolated in time from observed monthly mean fields in the period 1979-1993.

The computation has been performed in a computer (parallel run) with distributed memory VPP700.

For practical purposes, the analysis data corresponding to T106 truncation have been projected onto a Gaussian grid with 128 longitudes and 64 latitudes. A space domain ranging from 90°W to 90° E and from 20° to 80° N has been selected, so the domain comprises 65 longitudes and 22 latitudes. The Northern Hemisphere winter season has been taken as the 90-day period from 1 December to 28 February.

METHOD DESCRIPTION

The wavenumber spectral analysis and the power spectral analysis technique have been combined in the wavenumber-frequency spectral analysis or space-time spectral analysis. This not only includes conventional wavenumber and frequency spectral as special cases (Willson, 1975), but allows traveling waves to be distingued from fluctuating stationary waves. The use of such an analysis in studying the general circulation of the atmosphere, has shed new insights into the nature of large-scale atmospheric variability (Straus and Shukla, 1981; Pratt and Wallace, 1976) and has been extensively applied to data generated

by atmospheric models, in an attempt to determine the characteristics, structure and energetics of transient atmospheric waves (Hayashi, 1971, 1974, 1982).

Furthermore, this technique is an extension of space-time Fourier analysis which more properly treats the stochastic nature of atmospheric time series (Pratt, 1976; Fraedrich and Böttger, 1977; Hayashi, 1971). The underlying concept is the expression of atmospheric data in terms of basis functions, each of which corresponds to a wave of a particular zonal wavenumber and frequency.

Space-time spectral analysis is applied along a latitude circle at a given longitude-time series $q(\lambda,t)$ which is cyclic in longitude and limited in time (t). Total space-time variance may then be decomposed (Pratt, 1979), following Lorenz´s notation as

$$\overline{[q^2]} = \overline{[q]}^2 + \overline{[q^{*2}]} + \overline{[q]'^2} + \overline{[q'^{*2}]}$$
$$\qquad\quad A1 \qquad A2 \qquad A3 \qquad A4$$

where a square bracket designates a zonal average, the overbar represents a time average, the asterisk refers to zonal deviation (or the departure from zonal mean) and finally, the prime the departure from the time mean.

Terms A1, A2, A3 and A4 may be interpreted as follows: A1 is a squared spatial-temporal mean, A2 the variance of climatological stationary waves (forced by transients, heating and/or orographic contrasts), A3 the fluctuations of the zonal mean, and A4 the variance associated with combined space-time deviations. The last term informs about the interactions between scales of different wave-like phenomena, extremely important due to the highly nonlinear dynamics of the atmosphere (Doblas-Reyes, 1996). The space-time spectral analysis scheme we use follows the formulation of Pratt (1976). The procedure of computation involves the removal of zonal and time means from the data, calculation of zonal Fourier coefficients for each latitude and time and application of time cross-spectra.

The space-time variance of the transient waves (A4) is considered as one-sided in both wavenumber and frequency (Pratt, 1976) and is given by

$$T(k,\omega) = \frac{1}{2}\{P_\omega[C_k(t)] + P_\omega[S_k(t)]\}$$

Where P_ω is the power of the time series of the cosine $C_k(t)$ and sine coefficients $S_k(t)$ of the Fourier harmonics along a parallel of latitude. Unlike Hayashi formulations (1971, 1982) which is two-sided in frequency, the one-sided form combines the variance contribution from eastward, westward and zonally fixed fluctuations into one wavenumber-frequency component (total variance). Although the physical significance of $T(k,\omega)$ is clear (Pratt, 1979), we need measures of that part of total variance in each wavenumber-frequency category which results from zonally propagating or from the true standing motions.

A measure of standing (ST) wave variance is given by

$$ST(k,\omega) = \sqrt{K_\omega[C_k(t), S_k(t)] + \frac{1}{4}\{P_\omega[C_k(t)] - P_\omega[S_k(t)]\}}$$

where K_ω is the cospectrum which represents the interference between the eastward and westward components. Pratt (1976) and Hayashi (1977) defined the standing component as that part of the variance which describes eastward and westward moving component which are coherent with each other. Nevertheless, there is no unique partition of the space-time power spectra because of the non-orthogonality of the standing and traveling parts (Hayashi, 1971; Mechoso and Hartmann, 1982).

Propagating (PR) variance is the variance due to zonally propagating fluctuations and is defined as

$$PR(k,\omega) = |Q_\omega(C_k(t), S_k(t))|$$

where Q_ω is the quadrature spectrum of $C_k(t)$ and $S_k(t)$. The direction of propagation along a parallel of latitude is given by the algebraic sign of the quadrature and indicates which of the eastward and westward moving component is dominant. Positive (negative) values are indicative of eastward (westward) propagation.

Space-time spectral of the 500 hPa daily geopotential height have been computed at every latitude of the selected spatial domain. The spectral estimates are computed by using a lag-correlation method up to a 20-day lag. Smoothing is

accomplished by applying a Hamming window. The 14-spectra were averaged to obtain a mean estimate of the spectrum for every frequency-wavenumber pair.

Zonal wavenumber 1 through 7 are considered because we are interested in variability with scales greater than or equal to synoptic–scale transient eddies (≅ 1000 km). It must be taken into account that, on the following, the used wavenumber are half of the hemispheric zonal wavenumber, under an assumption of symmetry.

RESULTS

Zonal variance of the 500 hPa geopotential height stationary waves (Term A2)

The zonal variance of the geopotential height stationary waves in the model depicts a maximum around 50°N, notably smaller than in the analyses (Fig. 1a). This underestimation of the amplitude of stationary waves, which is associated to an excessive zonality of the flow constitutes, as was observed by different authors in previous studies one of the most common systematic errors in GCMs .

Time variance of the 500 hPa geopotential height zonal mean (Term A3)

The model maxima are located between 45°N-50°N and 65°N-70°N (Fig. 1b), and underestimate analysis values (Doblas-Reyes et al. 1998). This term has important consequences in the generation of blocking events due to its link to index cycle.

Analysis of the transient waves

Besides the study of different categories of the space-time spectral power, particular emphasis has been put on the low-frequency planetary waves region (k=1, $\nu < 0.15$ day^{-1}).

Total variance spectrum T(k,w)

The total variance spectrum for the transient waves depicts in both model and analyses, decreasing values with both frequency and wavenumber. As in Straus and Shukla (1981), a ridge of high spectral density extending from the low frequencies and small wavenumber to higher frequencies and wavenumbers is observed. Furthermore, an increase of power spectrum with latitude is detected in agreement with other authors (Madden, 1978; Willson, 1975; Pratt and Wallace, 1976). As expected (Pratt and Wallace, 1976) from the strong characteristic "redness" of meteorological time spectra, low-frequency oscillations may account for most of the variance. Values for model are, in general, weaker than in the analyses (Figures 2,3).

The total variance of low-frequency planetary waves (PLATOV) (Fig. 4a) shows an important underestimation of the model beyond 50°N, attaining 60% of the analyses value between 60° N and 70°N. As far as the latitudinal variation of total variance of synoptic-scale waves (not shown) is concerned, there is a big underestimation of the model which might be linked to the considerable underestimation of the planetary waves and the variance of the zonal mean north of 50°N.

It has been detected a different behaviour between the errors of the synoptic-scale and planetary disturbances which might be important due to symbiotic relationships between both types of disturbances (Vautard et al. 1988). Finally, in order to obtain a more detailed idea of the atmospheric variability, total variance frequency-spectrum for single wavenumbers (k=1 to k=5) have been calculated. Large-scale waves (k=1,2) have a large amount of low-frequency power and a very sharp drop in power with frequency. Shorter waves (k = 4,5) have less low-frequency power and have more slowly decreasing power with frequency. The wavenumber spectrum for ν = 0.025 day^{-1} depicts an underestimation of the model (k=1-4).

Standing spectrum ST(k,w)

The largest standing variance is found at both low frequency and wavenumber values, decreasing in an approximate radial way. The level of the standing variance in the model (Fig. 5) is lesser than in the analyses (Fig. 6). As can be seen, the standing variance spectra give the same kind of relationship that the total variance spectra. These results are in agreement with that of Fraedrich and Böttger (1978), Doblas-Reyes et al. (1998) Planetary standing variance (PLASTV) (Fig. 4b) in the analyses increases as a function of latitude, attaining the maximum at 65°N decreasing northward. Such latitudinal dependence is similar to the planetary total variance, which emphasizes the character mainly standing of the planetary waves in the selected hemispheric area. The model tends to underestimate the values.

The inability of the model to simulate in an appropriate manner the variance of the standing low-frequency planetary waves may be attributed to possible errors in the formulations of topographic and diabatic forcings.

Propagating variance spectrum PR(k,w)

Both analyses and model display a prevalence of eastward propagating waves while westward propagating waves are mainly restricted to low wavenumbers and frequencies. Pratt and Wallace (1976) have provided evidence that low-frequency planetary waves in the high midlatitudes can often be represented statistically as the combination of two independent modes of fluctuations.

For the analyses, the contribution of retrograde waves (k=1) turns out to be restricted to the frequency interval 0-0.1 day^{-1} , north of 40°N. Around 40°N, the interval is between 0.0-0.2 day^{-1}, which is the result of the superposition of a dominant westward component over an eastward component (Doblas-Reyes et al. 1998; Hayashi 1982; Pratt and Wallace 1976). South of 40°N, westward propagating waves has a core in k=1-2 and ν=0.05-0.25 day^{-1} (Fig.7), indicating the presence of another type of westward propagating waves where it will be

encompassed the 5-day south of 50°N described by Madden (1978). As for the model, the cores are less wide (north of 50°N) and a contribution at high wavenumbers has been detected (Fig. 8).

When observing -frequency spectra for single wavenumbers, an spectral peak for the westward propagating ultralong waves (k=1) at 45°N are restricted to periods 6.7-40 days (analyses) while for the model is at a period longer than 20 days. For k=2 to 5, there is eastward traveling variance in the analyses and a peak in k=3 and 10 days, being eastward traveling variance much stronger in the model.

The latitudinal distribution of propagative variance for planetary waves (PLAPRV) (Fig. 4c) shows in the analyses that the maximum in the westward variance which is found between 40°N-60°N is somewhat wider because the value attained at 40°N appears at 75°N.

The model is able to capture these retrograde waves, a very important and promising result with regard to the improvement of model simulation. They are detected, between about 37°N and 80°N, and one can talk about two maxima of variance around 45°N and between 65°N and 70°N. The maximum of eastward propagation is located between 30°N-35°N, being larger than the corresponding to the analyses. Doblas-Reyes (1998) worked with a previous version of the model and westward traveling fluctuations were not found except south of 40°N for the high resolution versions (T106 and T63). Kao and Lee (1977) pointed out a possible mechanism for the undersimulation of low-frequency planetary westward traveling waves in a GCM. They found that the interaction between stationary waves and moving planetary waves tend to supply energy to the westward mode and extract energy from the eastward mode. The problem in the stationary waves might be the reason that prevents retrograde waves to be created. Then, the improvement of these stationary waves in the new version may be a result of the better simulation of synoptic-scale transients, and thus of their forcing, could be one of the possible reasons why westward traveling waves in this version are sensibly better.

SUMMARY

In this study, we have put special emphasis on the behaviour of tropospheric intraseasonal westward traveling waves in the Euro-Atlantic region, making use of space-time spectral analysis. This version of the model is able to capture westward traveling waves, very stimulating result face to the model´s improvement.

ACKNOWLEDGEMENTS

We are indebted to the personnel at Météo-France for the use of the ARPEGE model. This work has been supported in part by the project CLI97-0558 (Comisión Interministerial de Ciencia y Tecnología, Spain).

REFERENCES

DÁndrea, F. and R. Vautard 2000. Reducing systematic errors by empirically correcting model errors. *Tellus* , 52 A, 21-41.

Déqué, M. and J. P. Piedelievre 1995. High resolution climate simulation over Europe. *Climate Dyn.*, **11**, 321-339.

Déqué, M., C. Dreveton, A. Braun and D. Cariolle 1994. The ARPEGE/IFS atmosphere model: a contribution to the French comunity climate modelling. *Climate Dyn.*, **10**, 249-266.

Doblas-Reyes, F. J., 1996. *El Bloqueo Atmosférico: Simulación en un Modelo de Circulación General y Patrones de Precipitación Asociados.* PhD Dissertation Universidad Complutense, Madrid, Spain, 289 pp.

Doblas-Reyes, F. J., M. Déqué, F. Valero and D. B. Stephenson, 1998. North-Atlantic wintertime intraseasonal variability and its sensitivity to GCM horizontal resolution. *Tellus*, **50A**, 573-595.

Doblas-Reyes, F. J. and M. Déqué, 1998.A flexible bandpass filtering procedure applied to midlatitude intraseasonal variability. *Mon. Wea. Rev.*, **126**, 3326-3335.

Fraedrich, K. and H. Böttger, 1978. A wavenumber frequency analysis of the 500 mb geopotential at 50°N. *J. Atmos. Sci.*, **35**, 745-750.

Hayashi, Y., 1971. A generalized method of resolving disturbances into progressive and retrogressive waves by space Fourier and time cross-spectral analysis. *J. Meteor. Soc. Japan*, **49**, 125-128.

Hayashi, Y., 1974. Spectral analysis of tropical disturbances appearing in a GFDL general circulation model. *J. Atmos.Sci.*, **31**, 180-218.

Hayashi, Y., 1977. On the coherence between progressive and retrogressive waves and a partition of space-time power spectra into standing and traveling parts. *J. Appl.Meteor.*, **16**, 368-373.

Hayashi, Y., 1982. Space-time spectral analysis and its apllications to atmospheric waves. *J. Meteor. Soc. Japan*, **60**, 156-171.

Hayashi, Y., and D.G.Golder, 1993. Tropical 40-50 and 25-30 day oscillations appearing in realistic and idealized climate models and the ECMWF dataset. *J. Atmos. Sci.*, **50**, 464-494.

Kao, S. K. and H. N. Lee 1977. The nonlinear interactions and maintenance of the large-scale moving waves in the atmosphere. *J. Atmos. Sci.*, **34**, 471-485.

Madden, R. A., 1978. Further evidence of traveling planetary waves. *J. Atmos. Sci.*, **35**, 1605-1618.

Mechoso, C.R. and D.L. Hartmann, 1982. An observational study of traveling planetary waves in the Southern Hemisphere. *J. Atmos. Sci.*, **39**, 1921-1935.

Pratt, R. W., 1976. The interpretation of space-time spectral qunatities. *J. Atmos. Sci.*, **33**, 1060-1066.

Pratt, R. W. and J. M. Wallace, 1976. Zonal propagation characteristics of large-scale fluctuations in the mid-latitude troposphere. *J. Atmos. Sci.*, **33**, 1184-1194.

Pratt, R. W., 1979. A space-time spectral comparison of the NCAR and GFDL General Circulation Models to the atmosphere. *J. Atmos. Sci.*, **36**, 1681-1691.

Speth, P. and R. A. Madden, 1983. Space-time spectral analyses of Northern Hemisphere geopotential heights. *J. Atmos. Sci.*, **40**, 1086-1100.

Straus, D. M.and J. Shukla 1981. Space-time spectral structure of a GLAS general circulation model and a comparison with observations. *J. Atmos. Sci.*, **38**, 902-917.

Vautard, R., B. Legras and M. Déqué 1988. On the source of midlatitude low-frequency variability. Part I: a statistical approach to persistence. *J. Atmos. Sci.*, **45**, 2811-2843.

Willson, M. A. G., 1975. A wavenumber–frequency analysis of large-scale tropospheric motions in the extratropical Northern Hemisphere. *J. Atmos. Sci.*, **32**, 478-488.

Figure captions

Fig. 1: (a) Latitudinal variation of the zonal variance of the 500 hPa geopotential height stationary waves for the analyses (solid line) and for the ARPEGE GCM simulation (short-dash line). (b) Same as (a) but for time variance of the geopotential zonal mean.

Fig. 2: Space-time total variance spectrum for the analyses at 4 selected latitudes (65°N, 60°N, 45°N, 30°N). Abscissa is frequency (day^{-1}) and ordinate is wavenumber. Units are m^2 .

Fig. 3: Same as Fig.2 but for the ARPEGE GCM simulation.

Fig. 4: (a) Latitudinal variation of the 500 hPa geopotential height total variance of the planetary low-frequency transient eddies for the analyses (solid line) and for the ARPEGE GCM simulation (short-dash line). (b) Same as (a) but for the standing variance of the planetary-scale low-frequency transient eddies. (c) Same as (a) but for the propagative variance of the planetary-scale low-frequency transient eddies. Negative values (westward propagation) are shaded.

Fig. 5: Logarithm of spectral power (10 m^2) of standing oscillations for the analyses at 4 selected latitudes (65°N, 60°N, 45°N, 30°N). Abscissa is frequency (day^{-1}) and ordinate is wavenumber.

Fig.6 : Same as Fig. 5 but for the ARPEGE GCM simulation.

Fig. 7: Logarithm of spectral power (10 m^2) of propagating oscillations for for the analyses at 4 selected latitudes (65°N, 60°N, 45°N, 30°N). Abscissa is frequency (day^{-1}) and ordinate is wavenumber. Regions with negative values (westward propagation) are shaded.

Fig. 8: Same as Fig. 7 but for the ARPEGE GCM simulation.

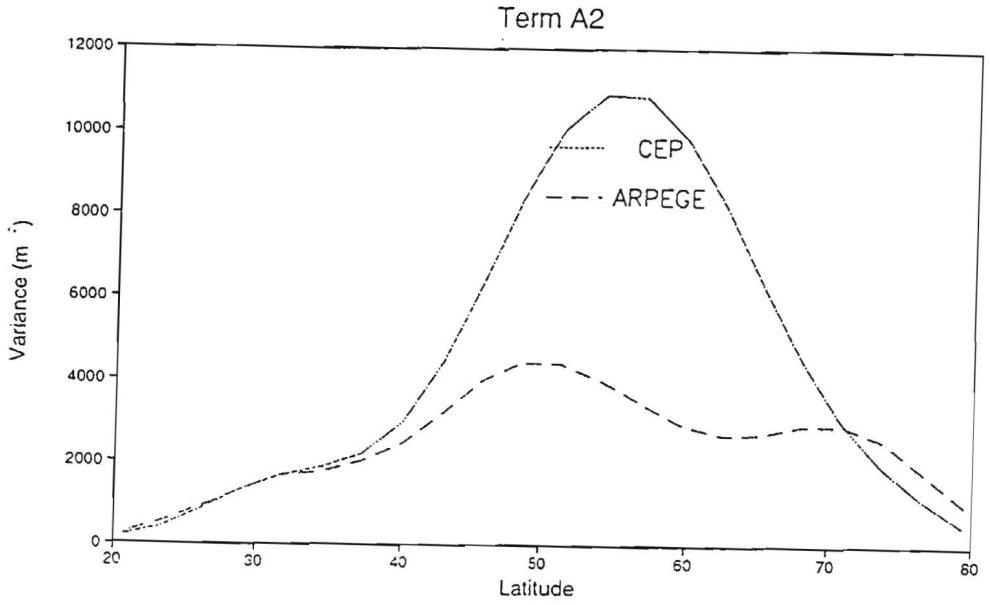
Term A2
12000
10000
8000
6000
4000
2000
0
Variance (m ²)
CEP
ARPEGE
20
30
40
50
60
70
80
Latitude

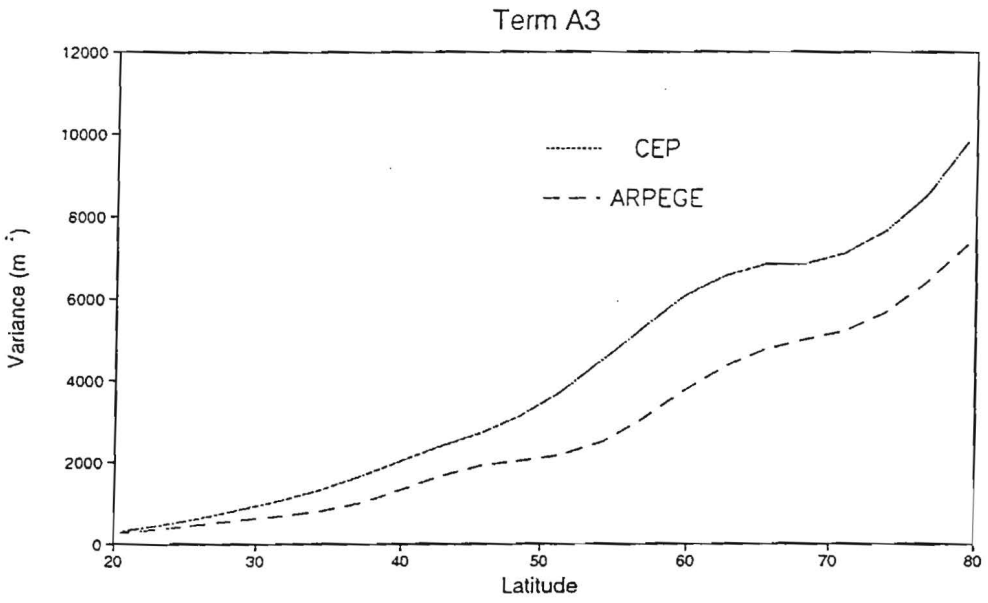
Term A3
12000
10000
8000
6000
4000
2000
0
Variance (m ²)
CEP
ARPEGE
20
30
40
50
60
70
80
Latitude

Figure 1

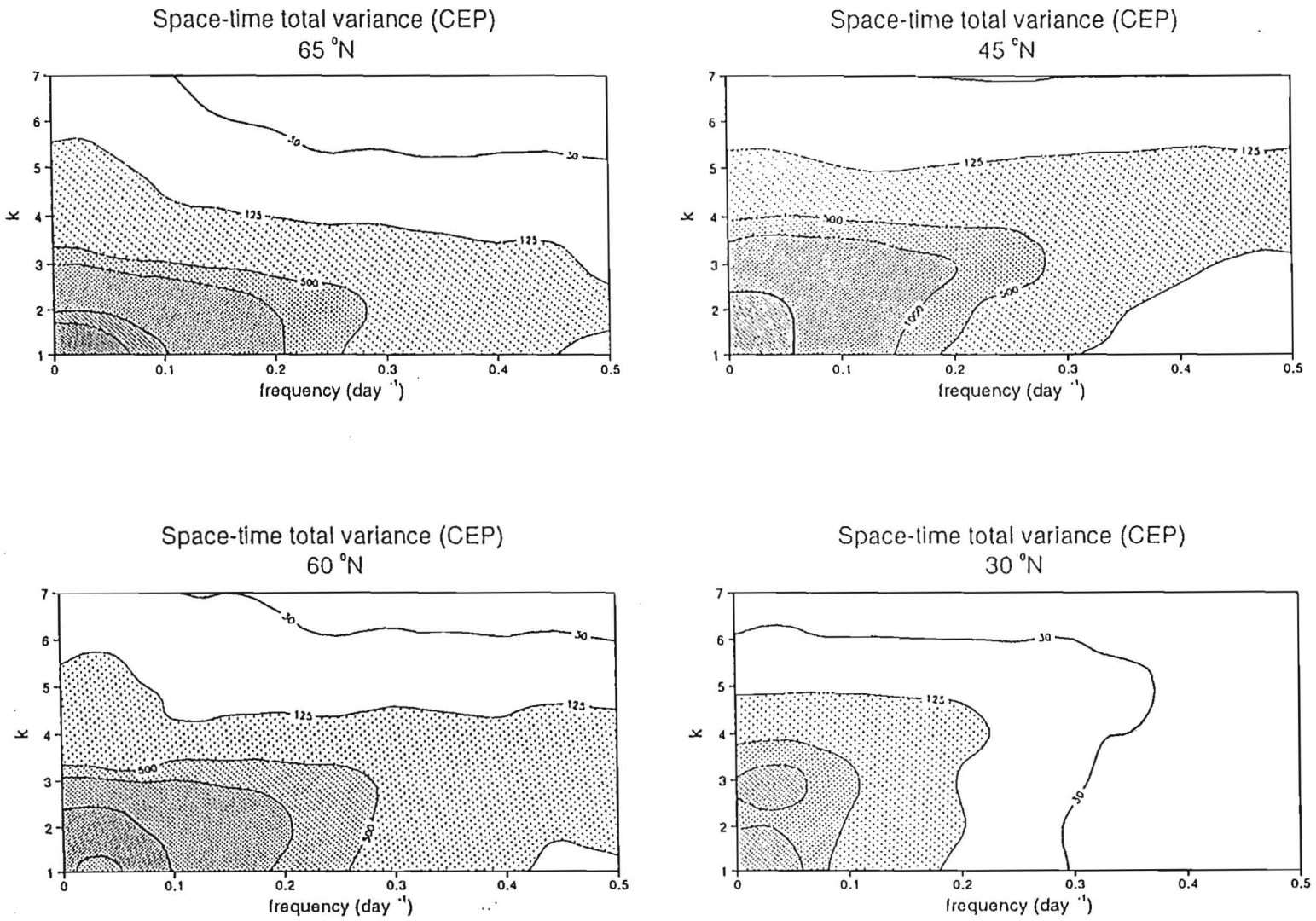
Space-time total variance (CEP)
65 °N
Space-time total variance (CEP)
45 °N
Space-time total variance (CEP)
60 °N
Space-time total variance (CEP)
30 °N
k
frequency (day -1)
30
125
500
1000

Figure 2

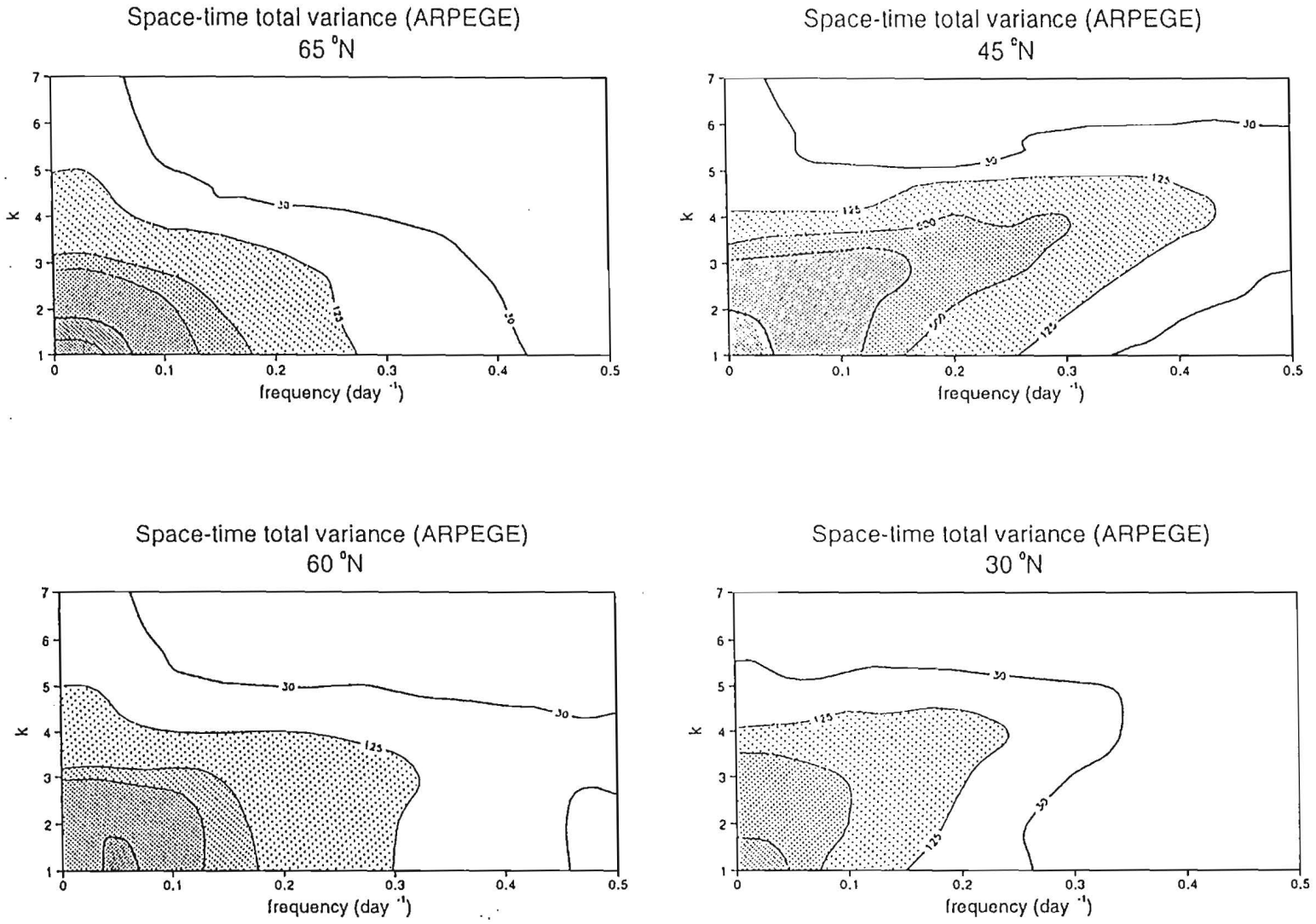
Space-time total variance (ARPEGE)
65 °N
Space-time total variance (ARPEGE)
45 °N
Space-time total variance (ARPEGE)
60 °N
Space-time total variance (ARPEGE)
30 °N
k
frequency (day -1)
0
0.1
0.2
0.3
0.4
0.5
1
2
3
4
5
6
7
30
125
250
270

Figure 3

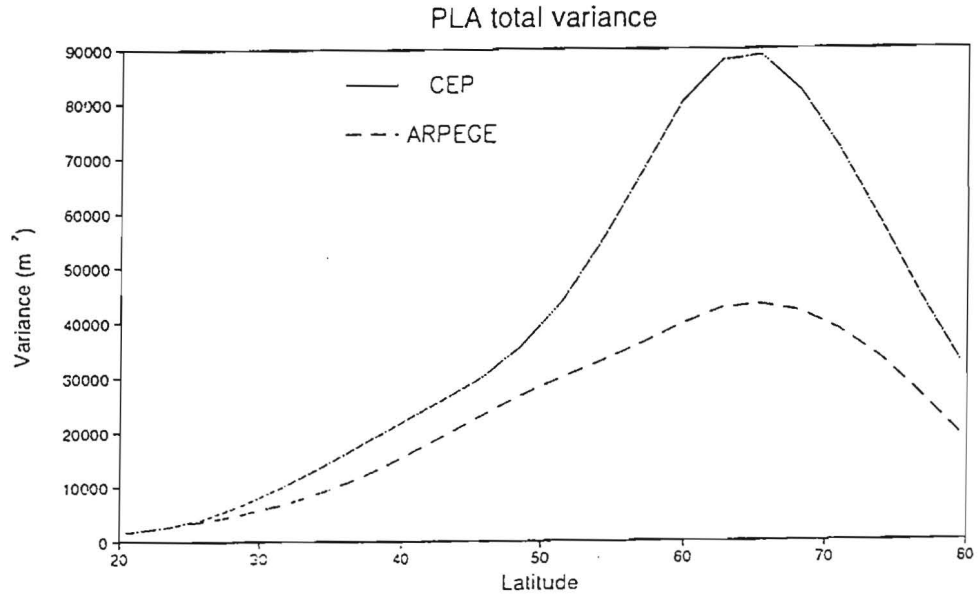
PLA total variance
CEP
ARPEGE
Variance (m ²)
Latitude

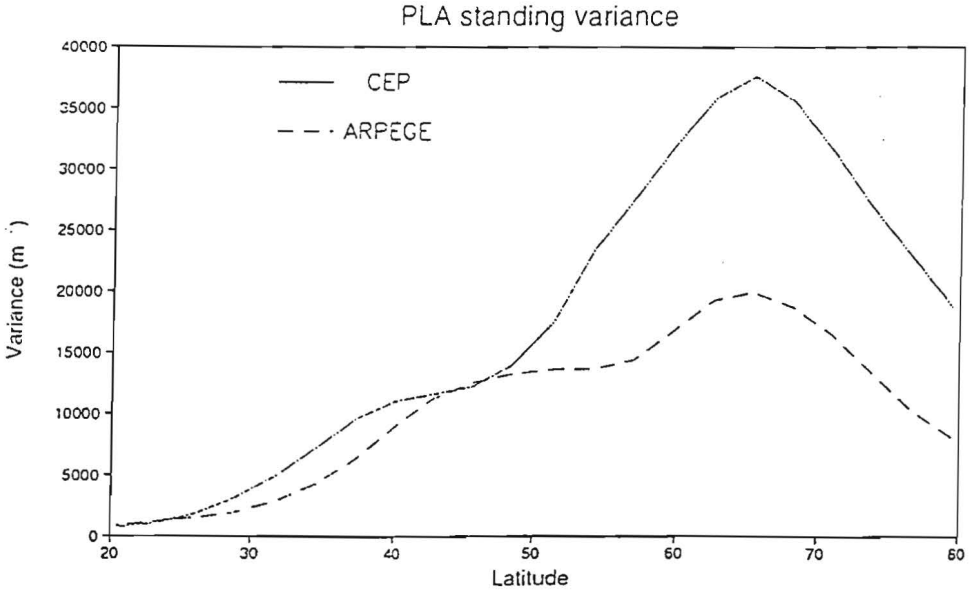
PLA standing variance
CEP
ARPEGE
Variance (m ²)
Latitude

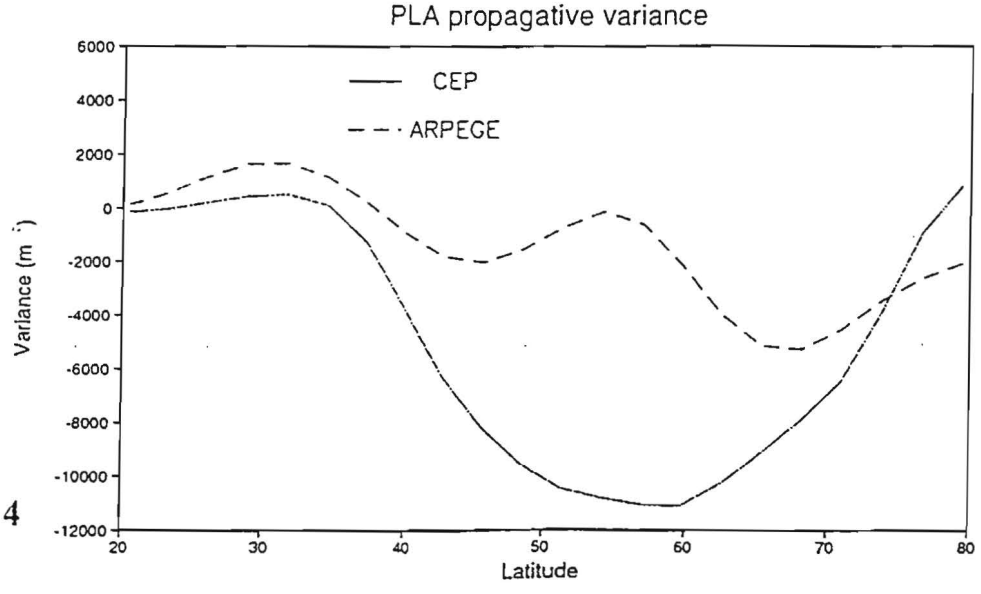
PLA propagative variance
CEP
ARPEGE
Variance (m ²)
Latitude

Figure 4

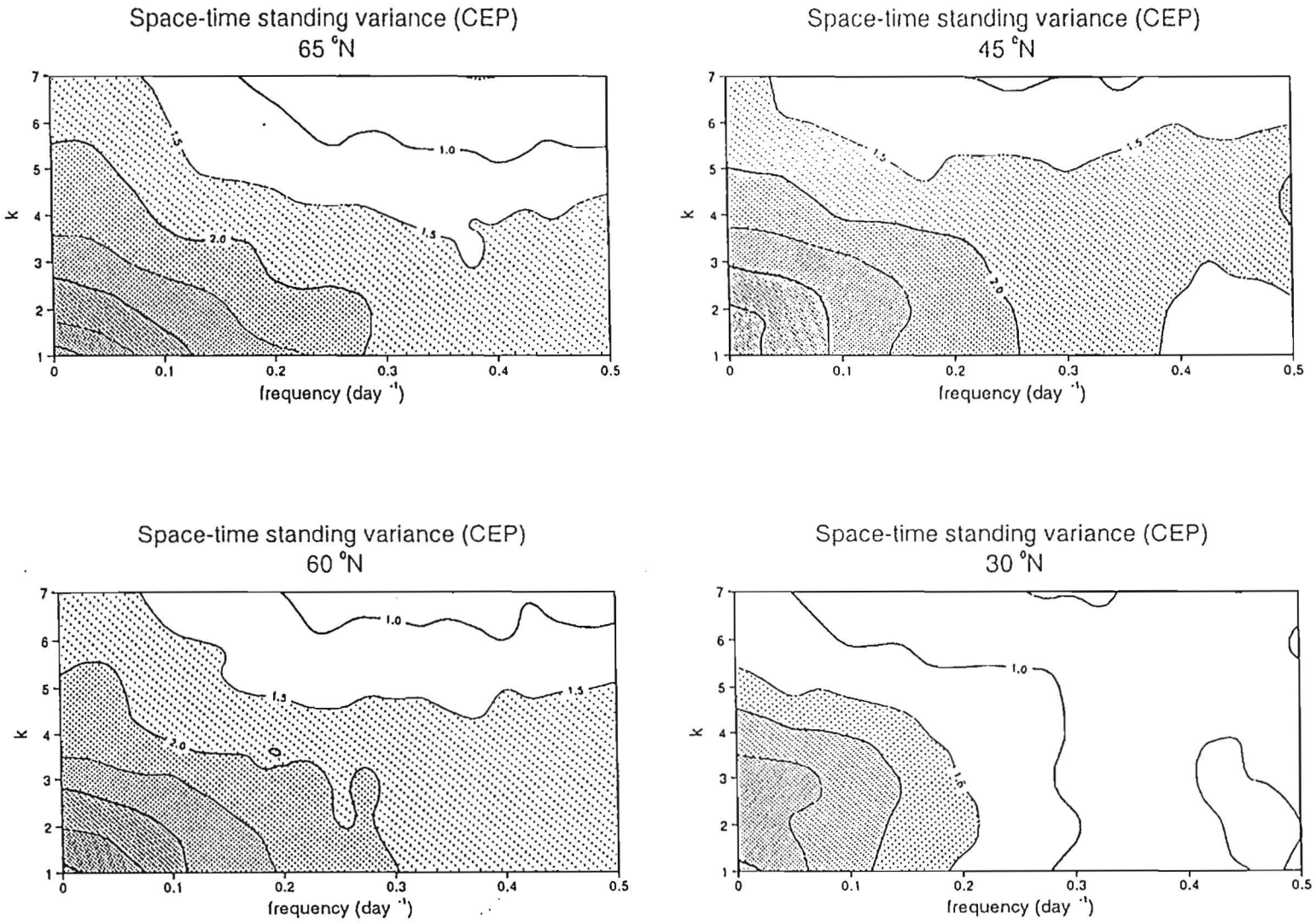
Space-time standing variance (CEP)
65 °N
Space-time standing variance (CEP)
45 °N
Space-time standing variance (CEP)
60 °N
Space-time standing variance (CEP)
30 °N
k
frequency (day -1)
1.0
1.5
2.0

Figure 5

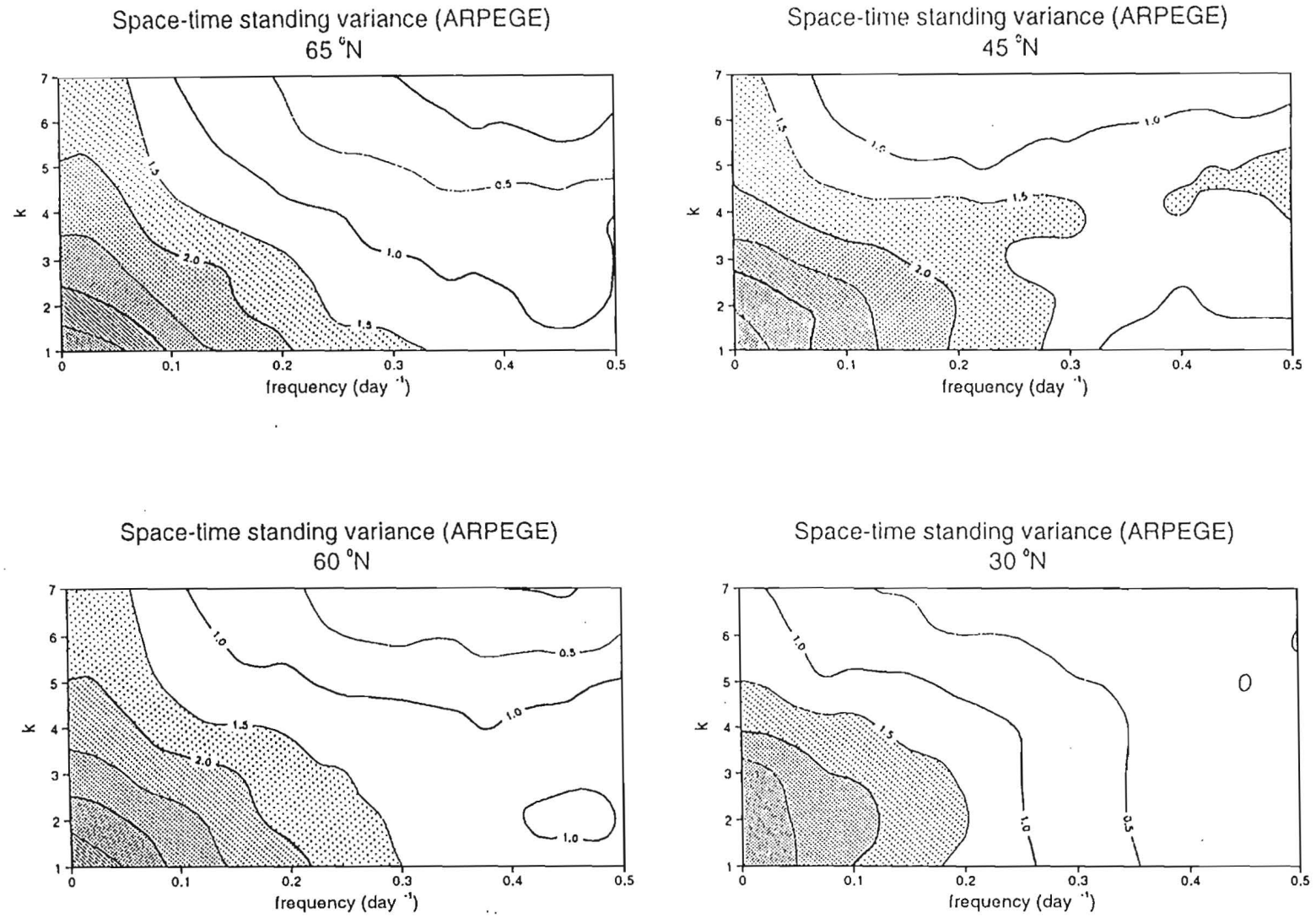
Space-time standing variance (ARPEGE)
65 °N
Space-time standing variance (ARPEGE)
45 °N
Space-time standing variance (ARPEGE)
60 °N
Space-time standing variance (ARPEGE)
30 °N
k
frequency (day -1)
0
0.1
0.2
0.3
0.4
0.5
1
2
3
4
5
6
7
0.5
1.0
1.5
2.0

Figure 6

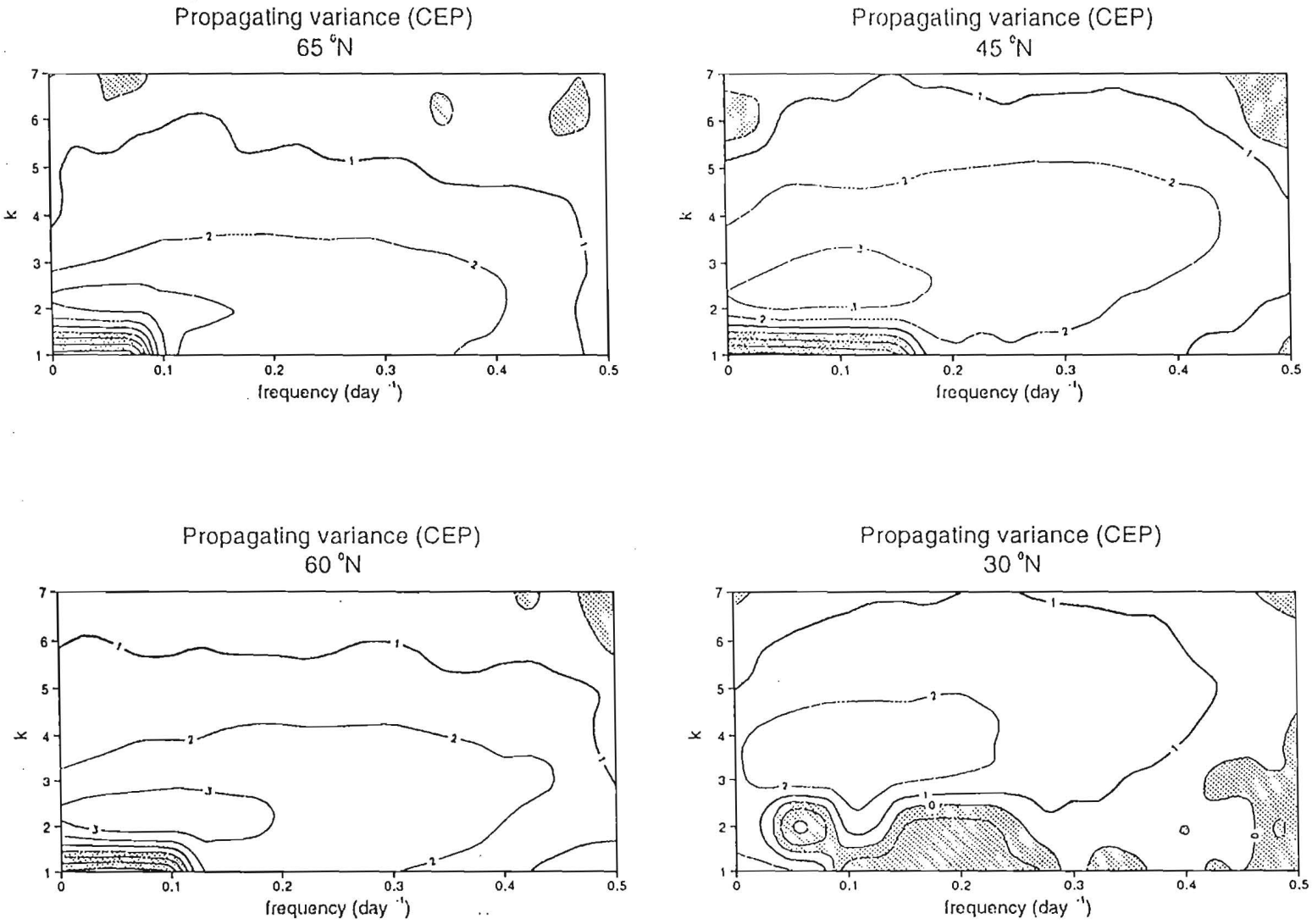
Propagating variance (CEP)
65 °N
Propagating variance (CEP)
45 °N
Propagating variance (CEP)
60 °N
Propagating variance (CEP)
30 °N
k
frequency (day -1)
0
0.1
0.2
0.3
0.4
0.5
1
2
3
4
5
6
7

Figure 7

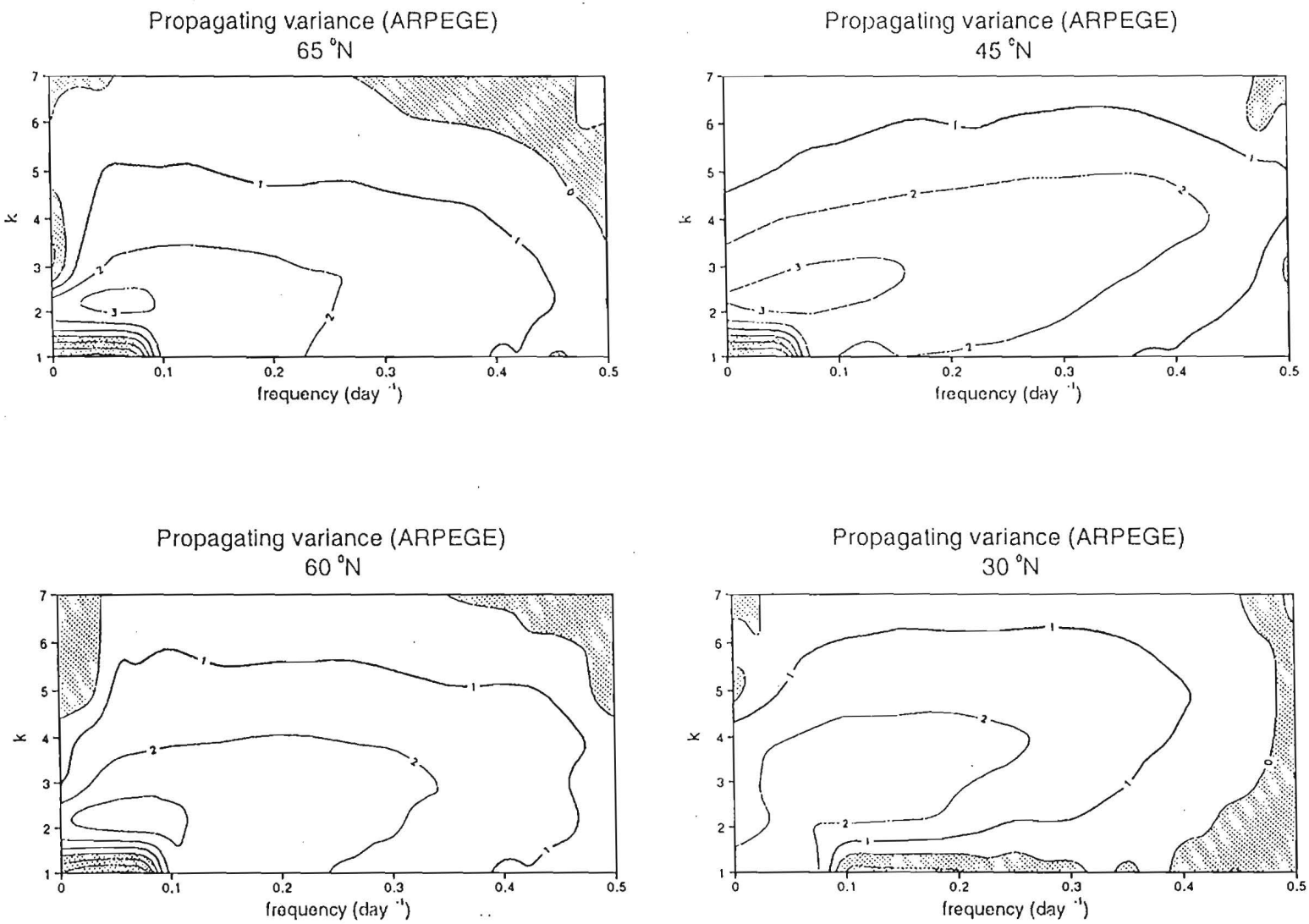
Propagating variance (ARPEGE)
65 °N
Propagating variance (ARPEGE)
45 °N
Propagating variance (ARPEGE)
60 °N
Propagating variance (ARPEGE)
30 °N
k
frequency (day -1)
0
0.1
0.2
0.3
0.4
0.5
1
2
3
4
5
6
7

Figure 8